We are IntechOpen,
the world's leading publisher of
Open Access books
Built by scientists, for scientists

6,900
Open access books available

186,000
International authors and editors

200M
Downloads

Our authors are among the

154
Countries delivered to

TOP 1%
most cited scientists

12.2%
Contributors from top 500 universities

Interested in publishing with us?
Contact book.department@intechopen.com

Numbers displayed above are based on latest data collected.
For more information visit www.intechopen.com

Chapter

Application of Artificial Neural Networks for Accurate Prediction of Thermal and Rheological Properties of Nanofluids

Behzad Vaferi

Abstract

Nanofluids have recently been considered as one of the most popular working fluid in heat transfer and fluid mechanics. Accurate estimation of thermophysical properties of nanofluids is required for the investigation of their heat transfer performance. Thermal conductivity coefficient, convective heat transfer coefficient, and viscosity are some the most important thermophysical properties that directly influence on the application of nanofluids. The aim of the present chapter is to develop and validate artificial neural networks (ANNs) to estimate these thermophysical properties with acceptable accuracy. Some simple and easy measurable parameters including type of nanoparticle and base fluid, temperature and pressure, size and concentration of nanoparticles, etc. are used as independent variables of the ANN approaches. The predictive performance of the developed ANN approaches is validated with both experimental data and available empirical correlations. Various statistical indices including mean square errors (MSE), root mean square errors (RMSE), average absolute relative deviation percent (AARD%), and regression coefficient (R^2) are used for numerical evaluation of accuracy of the developed ANN models. Results confirm that the developed ANN models can be regarded as a practical tool for studying the behavior of those industrial applications, which have nanofluids as operating fluid.

Keywords: artificial neural networks, solid-liquid suspension, nanofluids, thermal property, rheological property

1. Introduction

Increasing price of fuels as well as hardening the environmental regulations/laws enforces the industrial processes to increase the efficiency of their consumed energy. Therefore, concentrations are focused on the technologies that improve the performance of heat transfer equipment. This improvement is often achieved by either enhancing the thermophysical characteristics of the traditional operating fluids or modifying the structure of heat exchangers [1–3]. Unfortunately, conventional heat transfer fluids (e.g. water, engine oil, and ethylene glycol) suffer from inherently low thermal properties and poor heat transfer characteristics [4, 5]. Conducting research for modifying poor thermophysical properties of the

traditional fluids confirmed that adding solid particles to the base fluids can improve their heat transfer properties [6]. Since a solid metal has a larger thermal conductivity than a pure fluid, adding some of metallic solid particles in base fluids may improve their thermal behavior [7, 8]. Although, thermal conductivity of solid particle is typically an order-of-magnitude higher than the base fluid, adding micro-sized solid particles is not practically possible. The micro-sized solid particles that often simply settled down are responsible for some major problems including clogging the small passages, high pressure drop, and components erosion by abrasive action [9–12]. For solving these problems, most of the new studies have concentrated on synthesizing materials of nano-sized scale [9, 12]. Rapid progress of nanotechnology has motivated researchers to disperse various nanoscale particles (1–100 nm) in the operating fluids to form the new class of heat transfer fluid namely nanofluids [13–18]. The term of nanofluids was firstly proposed by Choi for addressing the homogeneous suspensions of nanoscale particles in base fluid [19]. Large relative surface area, higher heat conduction, excellent stability, and minimal clogging are the main advantages of nano-sized materials respect to micro-sized ones. It is possible to improve the thermophysical properties of the conventional fluids, and enhance their heat transfer ability by adding small amount of nano-sized solid particles [20]. It has been claimed that nanofluids are the best choice for the next generation of heat transfer fluids [5, 11].

Nanofluids have found high popularity due to their excellent ability in enhancement of heat transfer performances of various thermal systems during the recent years [16, 21, 22]. In spite of such potential benefits, nanofluid technology is still limited for commercial use as there are no proven standardized techniques for accurate prediction of important heat transfer characteristics of nanofluids [23, 24]. Availability of some accurate correlations/models for estimation of heat transfer characteristics of nanofluids is necessary during design, optimization, and control of those heat transfer devices that use these operating fluids. Therefore, in this chapter, great deals of efforts are made to correlate some thermophysical properties of nanofluids by artificial neural networks. In the next section, the procedure of working of artificial neural networks and four different types of ANN are briefly explained.

2. Artificial neural networks

Simulation of working procedures of the biological nervous system of the human brain is the basic idea for designing artificial neural networks [25]. Artificial neural network, as its name clearly implies is composed of some well-organized processing elements, namely neurons. Indeed, various types of these smart networks are constituted of a common processing unit namely artificial neuron or perceptron. The neuron has two regulating parameters that are often known as weight (w) and bias (b). The perceptrons receive their entry information from either other neurons or external source (x), and produces an output signal using Eq. (1).

$$out = f\left(\sum_{r=1}^{k} w_r x_r + b\right) \tag{1}$$

where *out* denotes the perceptron's output, and f is the activation function. ANN models often require different number of neurons in their layers for solving specific problems. Artificial neural networks can extract a function $g(\cdot) : R^{Ind} \rightarrow R^{Dep}$ by training on a dataset, where *Ind* and *Dep* indicate the number of dimensions for independent and dependent variables, respectively. Providing the ANN with a

databank of independent variables $X = [Ind_1 \, Ind_2 \cdots Ind_n]^T$ and their related dependent variable(s), their parameters can be tuned by a proper backpropagation training algorithm. In this way, it is possible to simulate the behavior of even the most complicated nonlinear systems with an acceptable accuracy often smaller than AARD = 10% [26, 27]. Activation functions are responsible for providing the artificial neural networks with nonlinear behavior. Different types of ANN paradigm have found high popularity as a technique for parameter estimation, pattern detection, data clustering, text processing, fault discovery, and so on [28].

2.1 Types of ANN model

In this chapter, four different types of artificial neural networks include multilayer perceptron (MLP), cascade feedforward (CFF), radial basis function (RBF), and generalized regression (GR) neural networks that are used as artificial intelligent techniques for characterization of thermophysical properties of nanofluids. These types of ANN model are briefly illustrated in the following four subsections.

2.1.1 Multilayer perceptron neural networks

The MLP is the most well-known feedforward approach that often has one or more hidden layers between dependent and independent variables. This type of ANN methodologies is used in the supervised learning process for the adjustment of its parameters. The term feedforward implies that the entry signals can only move inside the neural network from input layer toward an output layer. The backward flow for signal is not allowed in the MLP neural networks. The multi-layer perceptron constitutes of several layers of nodes including one input layer, one or more hidden layer(s), and one output layer. This type of ANN models has found high-reputation because of its excellent performances for handling of both regression and classification problems [25–27].

2.1.2 Cascade feedforward neural networks

By conducting some modifications on the topology of the multi-layer perceptron networks, Fahlman and Lebiere designed a new class of ANN namely cascade feedforward neural network [29]. They do their modification by providing the CFF neural networks with synaptic connections for neuron of each layer with neurons of all subsequent layers [30]. It has been claimed that convergence rate of learning process of the CFB model is better than other ANN topologies [31].

2.1.3 Radial basis function neural networks

RBF neural network has been structured as a two-layer feedforward neural network model [32]. In the hidden and output layer of the RBF approach, Gaussian and linear transfer functions are always used, respectively [32]. The radial basis neural network that originally developed by Broomhead and Lowe in 1988, is a powerful tool for interpolation among data in multi-dimensional problems [33, 34].

2.1.4 Generalized regression neural networks

The GR neural network that was firstly developed in 1991 by Specht is often viewed as a special reformation of the RBF model [35]. The main benefit of the GR paradigm is that its parameters can be easily adjusted during training stage.

Parameters of the general regression neural network can be simply tuned by only one-pass training with the sufficient number of experimental data.

2.2 Training of artificial neural networks

The training process is a well-established procedure that tries to adjust parameters of the ANN model, i.e., biases and connection weights. During the learning process, the ANN model is provided with a sufficient number of experimental data containing both independent and dependent variables of the considered phenomena. Thereafter, an appropriate training algorithm is employed to adjust the parameters of ANN model in such a way that it could predict the actual targets with acceptable accuracy. The training stage begins with random values for the weights and biases of ANN model. Thereafter, the numerical signals of independent variable (s) are fed to the artificial network and are made to flow through it until they reach the output layer. Finally, the output layer is responsible for producing the output signal(s). A training algorithm is then applied to minimize the difference between the actual and calculated values for dependent variable(s) by regulating the parameters of the ANN model. This adjustment continues as far as the deviation between calculated and actual target values reaches the predefined tolerance. As soon as the training stage is completed, the weights and biases are adjusted and they are kept unchanged. In this stage, it is possible to employ the trained ANN approach for estimating the dependent variable(s) from new independent datasets.

2.3 Performance analyses of artificial neural networks

Several statistical accuracy indices including MSE, RMSE, AARD%, and R^2 have been applied to investigate accuracy of various ANN models. Values of MSE, RMSE, AARD%, and R^2 are mathematically calculated by Eq. (2) to Eq. (5), respectively.

$$MSE = \sum_{i=1}^{N} \frac{\left(D^{\exp\cdot}(i) - D^{cal.}(i)\right)^2}{N} \tag{2}$$

$$RMSE = \left\{ \sum_{i=1}^{N} \frac{\left(D^{\exp\cdot}(i) - D^{cal.}(i)\right)^2}{N} \right\}^{0.5} \tag{3}$$

$$AARD\% = \frac{100}{N} \sum_{i=1}^{N} \left(\left| \frac{D^{\exp\cdot}(i) - D^{cal.}(i)}{D^{\exp\cdot}(i)} \right| \right) \tag{4}$$

$$R^2 = \frac{\sum_{i=1}^{N} \left(D^{\exp\cdot}(i) - \overline{\Delta D}\right)^2 - \sum_{i=1}^{N} \left(D^{\exp\cdot}(i) - \Delta D^{cal.}(i)\right)^2}{\sum_{i=1}^{N} \left(D^{\exp\cdot}(i) - \overline{\Delta D}\right)^2} \tag{5}$$

where D and N represent dependent variable and number of experimental data, respectively. $D_i^{\exp}$ is the experimental dependent variable, D_i^{cal} presents the value of ith predicted dependent variable by ANN model, and $\overline{\Delta D}$ is the average value of the experimental data points for dependent variable.

3. Characterization of properties of nanofluids by ANN approaches

In this section, different types on ANN are used for systematic estimation of thermophysical properties of nanofluids. The focus is concentrated on two thermal

and a rheological property of nanofluids. Thermal conductivity coefficient, convective heat transfer coefficient, and viscosity of nanofluids tried to be modeled by ANN approaches. For each parameter, experimental data and procedure of developing ANN model are collected, and evaluation of performance of the developed model is presented.

3.1 Thermal conductivity coefficient

Thermal conductivity of homogeneous dispersion of solid particles in liquids has its own importance for dozen of decades [36]. Since the uniform suspensions of nano-sized solid particles in liquids have better thermal characteristics than their associated base liquids, they may be considered as operating fluids for heat transfer systems [7, 9, 37–41]. Maxwell [36] and Hamilton and Crosser [42] proposed some basic correlations for the calculation of thermal conductivity of the homogeneous suspensions from their particle dosage, thermal conductivity of base fluids as well as particles. Moreover, effects of shape and size of nanoparticle, chemistry of base fluids, temperature, and pH on the level of enhancement of thermal conductivity of pure base fluids have been deeply investigated [39, 43, 44]. Some researchers observed that thermal conductivity of nanofluids is dramatically increased by increasing temperature [39, 43–46]. Brownian motion of nanoparticles is often considered as a key mechanism to explain enhancement of thermal conductivity of uniform dispersion of nano-sized materials in different base fluids [39, 44]. It is a widely accepted theory that Brownian motion has a direct relation with the fluid temperature and it increases by increasing temperature. Indeed, particle motions increase by temperature and it results in increasing the thermal conductivity of nanofluid [39]. Enhancement of thermal conductivity of nanofluids by increasing the suspension temperature has been reported by different groups of researchers [45–48]. Increasing concentration of nanoparticles in base liquids that increase the possibility of collisions between fluid molecules and solid particles can also improve the thermal conductivity of nanofluids. Influence of shape and size of nanoparticle on thermal conductivity of nanofluids was comprehensively studied by different groups of researchers [7, 9, 37, 45, 48]. It is worthy to be noted that the thermal conductivity of nanofluid was reported, which may be lower than the base liquids under some specific circumstances [45, 48].

3.1.1 Experimental data

Available correlations in the literatures approve that the thermal conductivity ratio (TCR) of alumina-water nanofluid has relationship with nanoparticle size, concentration of nanoparticle in base liquids, and temperature of suspension [39, 45–58]. Therefore, these parameters are considered as independent variables for the estimation of TCR of alumina water-based nanofluid using MLP network. As reported in **Table 1**, 280 experimental datasets for TCR of alumina-water nanofluids are collected from various literatures [39, 45–58]. The collected experimental data covers the fluid temperature ranging from 1 to 133.8°C, alumina nanoparticle size of 8–283 nm, volume fraction from 0.0013 to 0.16, and TCR values ranging from 0.99 to 1.2902.

There exists a well-known role of thumb that states the multi-layer perceptron neural networks with a single hidden layer can precisely learn a behavior of any multi-variable function with a desired tolerance [22]. Therefore, in this section, a MLP network is structured with only one hidden layer to predict thermal conductivity ratio of the alumina-water nanofluid. Number of hidden neurons has been selected using trial and error procedure on minimizing both MSE and AARD%, and maximizing R^2 values for training as well as testing datasets. **Table 2** reports

Temperature range (°C)	Nanoparticle volume fraction	Nanoparticle diameter (nm)	Thermal conductivity ratio	N^*	References
21–51	0.01–0.04	38.4	1.02–1.242	12	[39]
21–71	0.01–0.04	11–150	1.01–1.2902	34	[45]
27.5–34.7	0.02–0.1	36	1.077–1.1513	22	[46]
21–60	0.01	80–150	1.033–1.106	10	[47]
10–50	0.0013–0.0052	20–100	1.004–1.147	36	[48]
20–40	0.031–0.09	36	1.157–1.259	30	[49]
1–40	0.01–0.04	30	0.99–1.219	15	[50]
10–60	0.05	40	1.096–1.128	6	[51]
10–50	0.03–0.16	20	1.06–1.214	12	[52]
15–60	0.01–0.08	120	1.025–1.257	30	[53]
20–60	0.03–0.13	30–80	1.041–1.257	24	[54]
23.5–27.4	0.0186–0.04	8–283	1.0214–1.185	21	[55]
24–133.8	0.01–0.04	12	0.99–1.228	24	[56]
35.5	0.0033–0.03	36	1.015–1.096	5	[57]
20	0.005–0.06	43	1.063–1.28	4	[58]

Number of experimental data.

Table 1.
Physical and operating conditions of various experimental datasets.

numerical values for the observed MSE and AARD% between calculated TCRs and their associated experimental data. It should be mentioned that the only difference between these MLP models is the number of hidden neurons. For reducing the effect of random selection of weights and biases on the final results, all of the MLP models are trained and tested 10 different times, and only the best obtained results for each topology is reported in **Table 2**. Indeed, in this section, we checked 200 MLP paradigms to find the best one.

3.1.2 Development of ANN model

It can be simply understood from **Table 2** that predictive performance of the MLP for the training subset is improved by increasing the number of hidden neurons. The AARD% for MLP model having 1–20 hidden neurons continuously decreases from 4.24 to 0.91%. But, performance of the MLP approach for estimation of the testing dataset only improves up to 14 hidden neurons, and thereafter no impressive progress is observed. It can be concluded that increasing the hidden neurons more than 14 only enlarges the MLP networks and has no positive effect on improving the accuracy [59]. Therefore, by considering the reported results in **Table 2**, a MLP approach with single hidden layer having 14 neurons (the bold row) is selected as the best structure for estimation of thermal conductivity ration of alumina-water nanofluid. This optimal MLP model is capable to estimate the testing dataset by MSE and AARD% of 6.3×10^{-4} and 1.75%, respectively.

This optimal MLP paradigm provides excellent R^2 values between the predicted and the actual values of TCR for both training and testing dataset. The calculated values of R^2 for the MLP models with 1–20 hidden neurons are depicted in **Figure 1**.

Number of hidden neuron*	AARD%		MSE	
	Training	Testing	Training	Testing
1	4.24	4.42	0.004542	0.004210
2	3.86	3.48	0.003877	0.003723
3	3.48	4.06	0.003397	0.004666
4	3.04	3.51	0.002563	0.003569
5	2.94	2.97	0.002171	0.001974
6	2.41	3.06	0.001696	0.002183
7	1.81	2.97	0.000736	0.002246
8	2.39	3.22	0.001295	0.002848
9	1.75	2.79	0.000681	0.003002
10	1.66	1.83	0.000687	0.001031
11	1.78	1.92	0.000781	0.000741
12	1.37	2.43	0.000429	0.001689
13	1.14	2.64	0.000345	0.002499
14	**1.23**	**1.75**	**0.000330**	**0.000630**
15	1.11	1.94	0.000303	0.001152
16	1.02	2.14	0.000273	0.00139
17	1.14	2.76	0.000343	0.002737
18	1.07	2.67	0.000354	0.003447
19	1.28	2.45	0.000484	0.002184
20	0.91	2.16	0.000201	0.001754

The best obtained results among 10 various trained network per each topology.
The bold values indicate the best obtained results for the considered AI models.

Table 2.
Evaluation of the best topology of the MLP model.

The values of observed AARD% and MSE by MLP models with different numbers of hidden neurons for the overall dataset (training + test) are shown in **Figure 2**.

To simulate behavior of a given system by the MLP neural network, a relatively huge amount of experimental data is required. **Figure 3** depicts variation of observed mean square errors (between MLP predictions and actual data of TCR of alumina-water nanofluids) as function of the number of epoch. As mentioned earlier, the procedure of adjustment of weights and biases of the MLP model is done by an optimization technique namely training algorithm. It is obvious that the optimization technique tries to minimize the observed MSE by an iteration procedure. In **Figure 3**, the term of epoch shows the number of interactions that the training algorithm has tried to tune the MLP parameter using the given procedure in Section 2.2. It can be seen from **Figure 1** that by increasing the number of iterations (i.e. epoch), weights and biases of the MLP model converge to their optimized values, and therefore, the observed MSE continuously decreases. After 800 iterations, the training algorithm enforces the MSE to converge 3.3×10^{-4}. Since this level of MSE between predicted and actual values of TCR is relatively small value, it can be said that the training was successful.
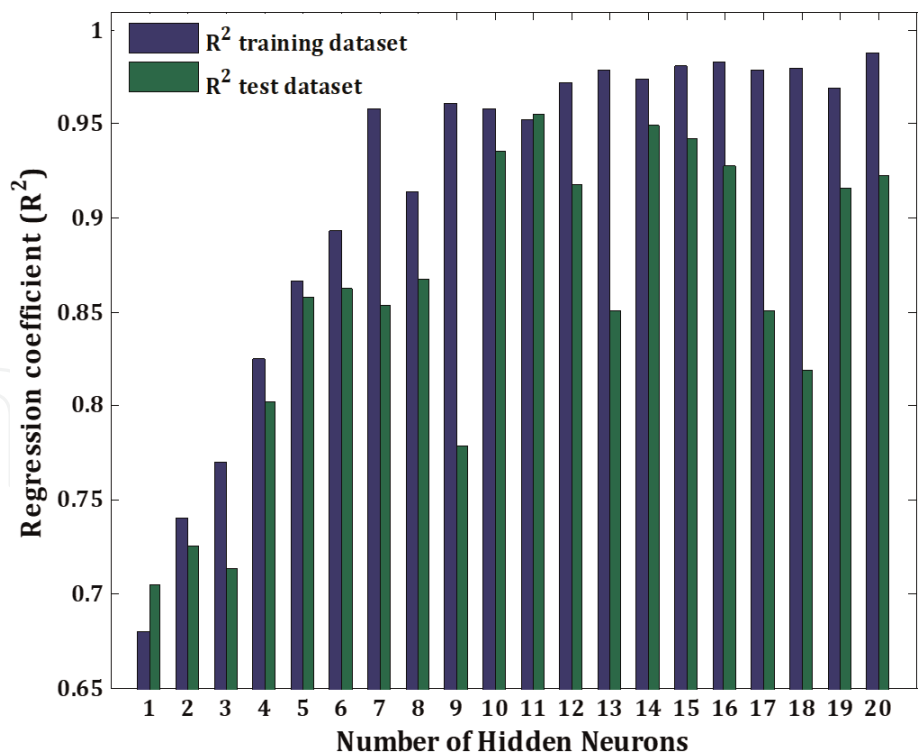
Figure 1.
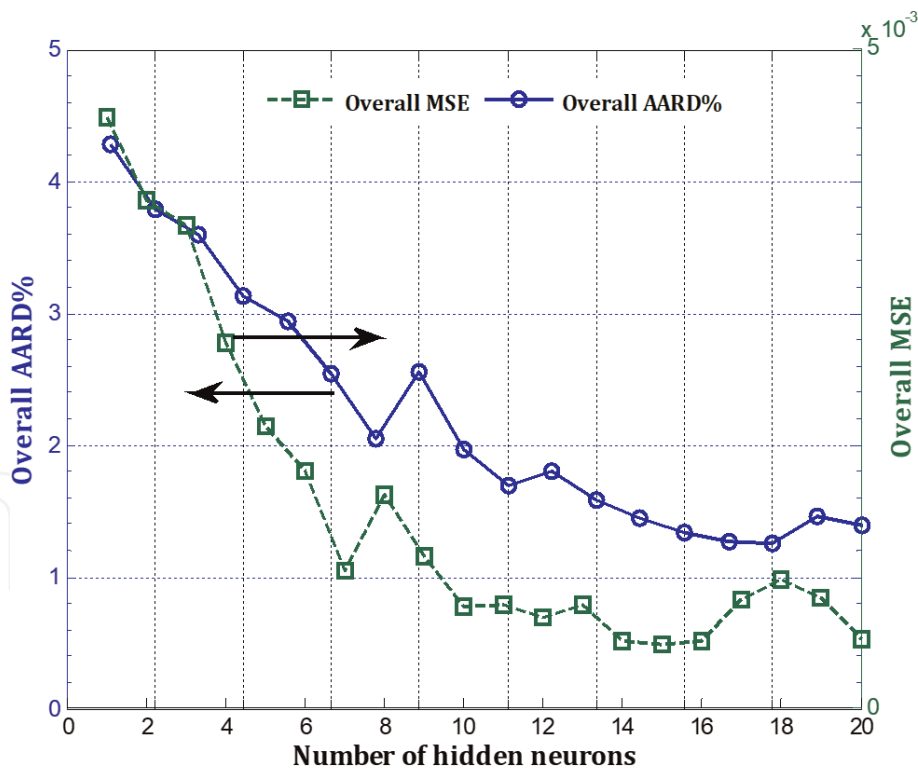*R² values of the proposed model for training and testing subsets.*

Figure 2.
Overall AARD% and MSE of various ANN models over training and testing subsets.

3.1.3 ANN model evaluation

A databank with 228 experimental datasets for TCR of water-alumina nanofluids has been collected from different literatures [39, 45–58]. These datasets have been used to design and validate the accuracy performances of different MLP networks as well as to find the best topology of the MLP model. Moreover, 57 experimental

TCR data-points, which were not utilized in the training process have been used to check the predictive accuracy of the proposed MLP paradigm.

In this part, performance of the proposed MLP approach tried to be evaluated by plotting the predicted values of TCRs as function of their associated experimental values for both testing and training subsets. **Figure 4** confirms an excellent performance and remarkable accuracy of the optimal MLP model for the estimation of experimental values of TCR of water-alumina nanofluids for overall databank. The most exact prediction (calculated TCRs = experimental data) is shown by a solid dashed 45° line. A relatively large $R^2 = 0.971875$ that observed for predicting all the experimental TCRs justifies that there is an excellent agreement between the predications of MLP model and the actual experimental data.
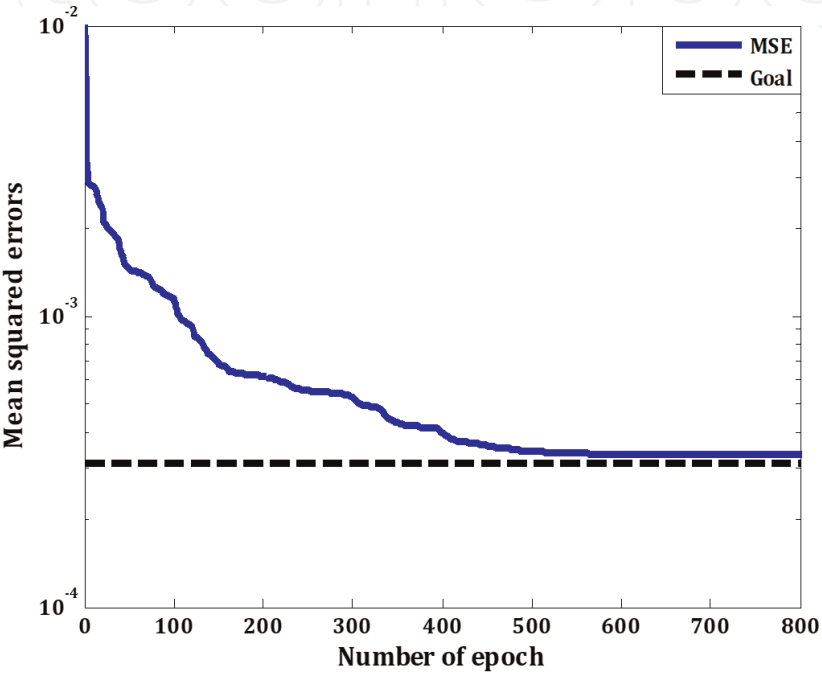

Figure 3.
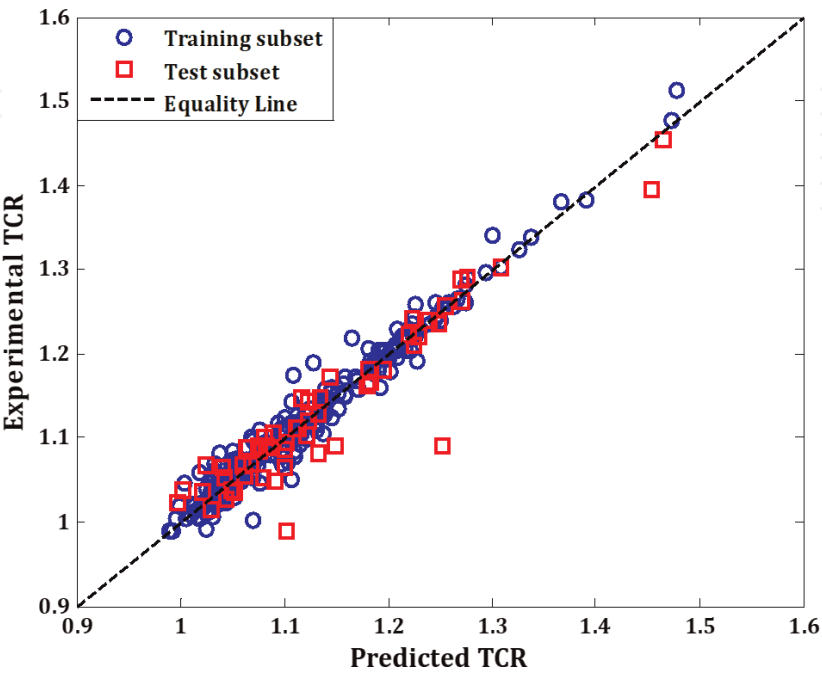*Variations of the mean squared errors with epoch during MLP training.*

Figure 4.
Predicted thermal conductivity ratio vs. measured ones for the overall dataset.

Table 3 summarizes an accuracy of the optimal MLP model with the six well-known empirical correlations for prediction of experimental data reported by Das et al. [39, 45, 47, 49, 60–62]. This table shows that the proposed MLP model presents the best overall AARD of 0.866% for the considered experimental data. The proposed model by Chon et al. [45] provides an AARD = 1.331% that is the best results among the considered correlations.

Table 4 reports results of estimation of experimental TCR data reported by Chandrasekar et al. [57] using our smart model as well as various empirical correlations [45, 47, 49, 60–62]. It can be simply seen that our proposed MLP model predicts the experimental data with the smallest deviation (AARD = 0.117%). The proposed correlations by Yu and Choi [60] and Xie et al. [61] that provide relatively similar results (AARD = 0.39%) are the best empirical correlations.

3.2 Convective heat transfer coefficient

It is obvious that a convective heat transfer coefficient (HTC) of nanofluids depends on concentration of the dispersed nanoparticles, their shape and size, flow structure, thermal conductivity and heat capacity of both nanoparticles and base liquid, and viscosity of nanofluid. Generally, addition of nanoparticles to the base liquid improves its thermal conductivity. Increasing an amount of energy transfer by the liquid leads to a higher temperature gradient between tube wall and bulk of nanofluid. It is a reason that is often highlighted for explanation is an increasing rate of convection heat transfer between nanofluid and tube wall [63].

Volume fraction of Al$_2$O$_3$	The considered intelligent approach and empirical correlations							
	Chon et al. [45]	Murshed et al. [47]	Mints et al. [49]	Yu and Choi [60]	Xie et al. [61]	Nan et al. [62]	MLP model	Actual TCR [39]
0.01	1.09	1.08	1.02	1.03	1.03	1.03	1.10	1.111
0.02	1.15	1.16	1.04	1.07	1.07	1.06	1.14	1.141
0.03	1.20	1.25	1.05	1.10	1.10	1.09	1.16	1.170
0.04	1.24	1.34	1.07	1.14	1.14	1.12	1.26	1.241
AARD%	1.331	4.818	10.270	6.909	6.909	7.744	0.866	—

Table 3.
Comparison among accuracy of various approaches for the prediction of experimental TCRs measured by Das et al. [39] (T = 51°C, Dp = 38.4 nm).

Volume fraction of Al$_2$O$_3$	The considered intelligent approach and empirical correlations							
	Chon et al. [45]	Murshed et al. [47]	Mints et al. [49]	Yu and Choi [60]	Xie et al. [61]	Nan et al. [62]	MLP model	Actual TCR [57]
0.003	1.0136	1.0253	1.0058	1.0117	1.0118	1.0097	1.0145	1.015
0.0075	1.0220	1.0594	1.0136	1.0230	1.0231	1.0214	1.0306	1.031
0.010	1.0331	1.0818	1.0175	1.0341	1.0343	1.0292	1.0316	1.032
0.020	1.0545	1.1646	1.0351	1.0672	1.0673	1.0584	1.0750	1.074
0.030	1.0760	1.2523	1.0516	1.1023	1.1025	1.0896	1.0920	1.096
AARD%	0.587	3.406	1.524	0.388	0.386	0.635	0.117	—

Table 4.
Comparisons of the predictive accuracy of different smart and empirical correlations over experimental TCR measured by Chandrasekar et al. [57] (T = 35.5 °C, Dp = 36 nm).

The objective of this part of chapter is to design a smart approach based on artificial neural networks for accurate estimation of convective HTC of different nanofluids flowing inside circular tubes. The great deals of effort are made to predict the HTC of nanofluids from the easily measurable characteristics of a system. Correlation matrix analysis approves that size of nanoparticles, their molecular weight (Mw) and volume concentration fraction (V_f), critical pressure and temperature of the base fluids (Pc and Tc), their acentric factor (ω), Reynolds number (Re), and the wall condition are the most important factors that influence on the convective HTC of nanofluids. It should be mentioned that we consider two different conditions for tube wall including uniform heat flux and constant temperature. From practical point of view, these two conditions are often encountered in various industrial applications.

The major part of the current section is dedicated to find the best ANN type as well as its topology for the considered task. Indeed, the ANN type with the smallest size that could provide the most accurate results for estimation of HTC of nanofluids is considered as the best topology. After evaluating the most accurate ANN type and its topology, we tried to compare its prediction results with available empirical correlations in different literatures.

3.2.1 Experimental databank

For the convective HTCs, 346 experimental data which covered the Reynolds number 600–8.9 $\times$ 10^4 and nanoparticle size of 20–100 nm are collected from different literatures [64–68]. The considered physical properties and their ranges as well as minimum-maximum values of convective HTCs of the collected experimental data, which collected from various literatures are presented in **Table 5**. These experimental data are used for developing ANN models and validating their predictive capabilities.

3.2.2 Designing an ANN model

All the experimental datasets have been randomly allocated to two different subsets namely train and test subsets. These two subsets have different application

Nanofluid	Nanoparticle size (nm)	Heat flux (W/m^2)	Temperature, Range (K)	Vf, Range (%v)	Re	h (W/m^2 K)	N*	Reference
Al$_2$O$_3$/Water	45	8842	—	0.25–1.5	600–2200	600–2000	58	[64]
Water	—	8842	—	—	900–2100	500–800	6	[64]
Al$_2$O$_3$/EG-W	45	218,000	—	2–10	3000–15,000	8000–19,000	57	[65]
SiO$_2$/EG-W	20, 50, 100	218,000	—	4, 2	3000–15,000	6000–19,000	37	[65]
CuO/EG-W	29	218,000	—	4	3000–12,000	8000–18,000	10	[65]
EG-W	—	218,000	—	—	4000–17,000	5000–16,000	11	[65]
Al$_2$O$_3$/Water	40	—	20–60	0.1–2	3000–18,000	2000–13,000	76	[66]
Water	—	—	20–60	—	3000–18,000	2000–11,000	17	[66]
Fe$_3$O$_4$/Water	36	12,489	—	0.02–0.6	3000–22,000	2000–49,000	51	[67]
Water	—	12,489	—	—	3000–22,000	900–8000	13	[67]
EG-W	—	500,000	—	—	10,000–89,000	7000–38,000	10	[68]

*Number of experimental data.

Table 5.
Physical and operational conditions of various datasets.

in the development of ANN model. Indeed, the training datasets have been used for adjusting weights and biases of the ANN approach as well as selecting its best structure. On the other hand, the predictive performance of this trained ANN model is often validated by the testing subsets. Since the testing datasets are not used during training stage and the ANN model did not see them previously, they could be considered as a reliable benchmark for evaluation/validation performance of the model in the unknown situations.

Various ANN types including RBF, MLP, CFB, and GR neural network are checked and the best one is selected based on its predictive capabilities. The optimal size of ANN approach (number of hidden neurons) is the smallest network, which can predict both train and test subsets within an acceptable error.

In this section, an iterative constructive method is used for determination of an optimal numbers of hidden neurons. Iterative constructive method increases the number of neurons in hidden layer gradually as long as a testing error be fixed or begins to rise. Values of observed AARD% for estimation of both testing and overall experimental data for 20 different MLP models that have 1–20 neurons in their hidden layer are presented in **Figure 5**. It can be simply understood from **Figure 5** that the testing errors are decreased by increasing the number of hidden neurons up to 10. Thereafter, no significant reduction in AARD% can be seen. Accordingly, the single hidden layer MLP approach having 10 hidden neurons is selected as the best structure for estimation of convective HTC of six different nanofluids and five considered pure liquids.

Values of the R^2 and MSE between experimental convective HTC and those HTC values predicted by various MLP networks are presented in **Figures 6** and 7, respectively. It can be seen from these figures, the 10 hidden neurons that present the largest value for R^2 as well as the smallest value for MSE over huge experimental databank can be regarded as the optimum value. It is worthy to be mentioned that vertical axis of **Figure 6** is in logarithmic scale to magnify increasing trend of MSE after 10 hidden neurons. The observed MSE for estimation of the testing datasets decreases by increasing the number of hidden neurons up to 10. After that no notable improvement in expense of enlarging the MLP model can be found. It can
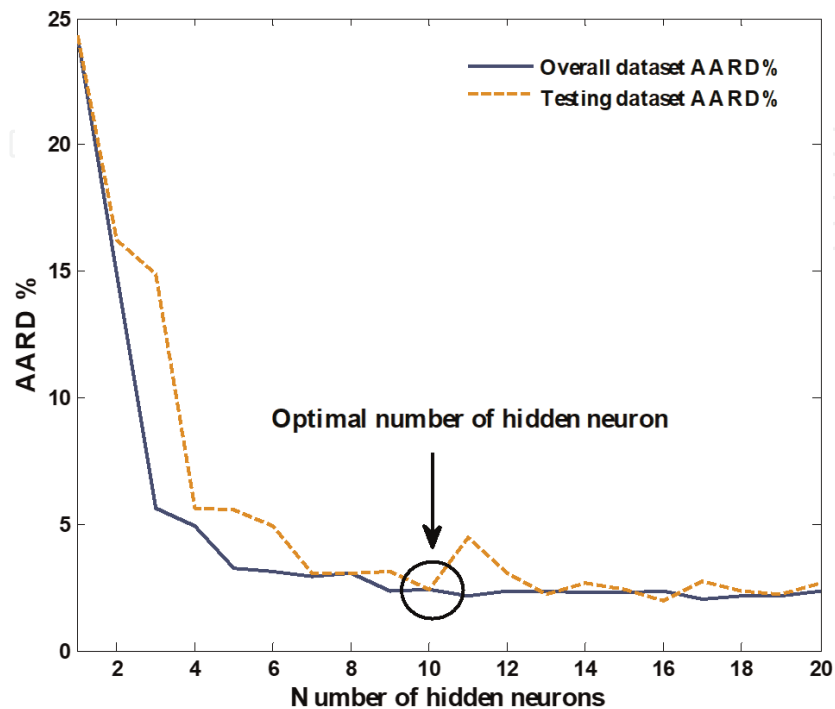

Figure 5.
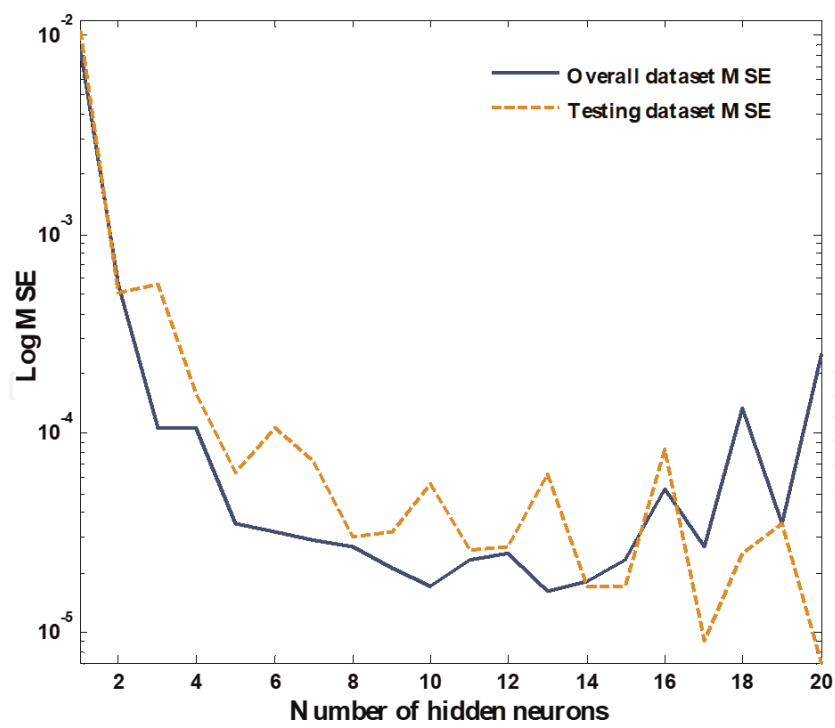*AARD% of various MLP topologies for testing and overall subsets.*

Figure 6.
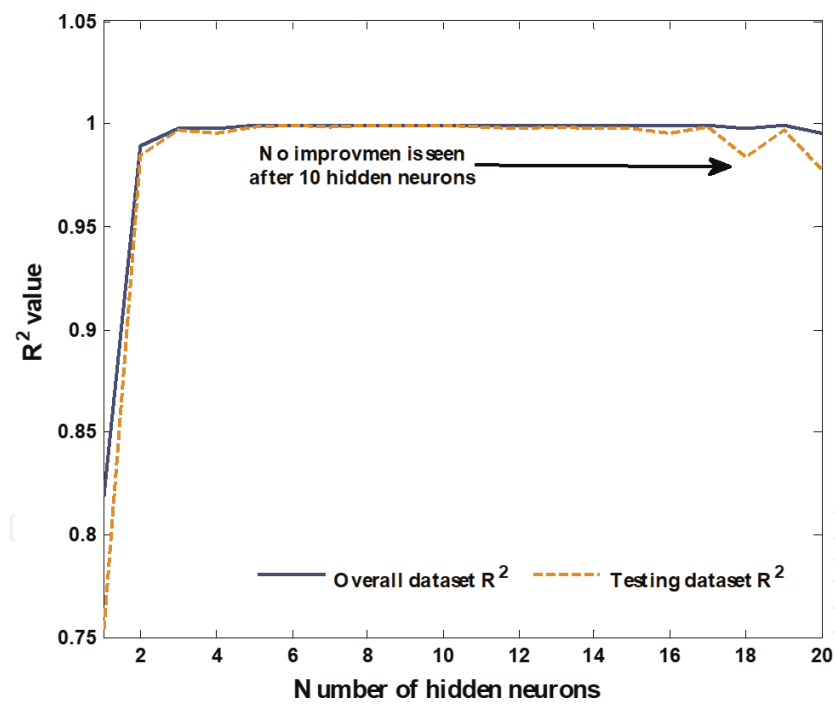*MSE logarithm of various ANN topologies for testing and overall sets.*

Figure 7.
Associated R² values of ANN topologies for testing and overall sets.

be said that using more than 10 hidden neurons for the MLP models not only increase the size of the model but it has no positive effect on reducing the magnitude of the errors.

Here, we tried to do some comparisons between predictive performance of the optimum MLP model with other available feedforward neural networks, i.e., radial basis, cascade feedforward, and generalized regression neural networks. **Table 6** summarizes the result of four smart models for simulation of the behavior of convective HTC of different pure fluids and nanofluids. It should be mentioned that all of these four intelligent models, i.e., MLP, RBF, GR, and CFF neural networks

ANN model		Accuracy indices		
		MSE	AARD (%)	R^2
Multi-layer perceptron neural network	Train subset	0.000016	2.63	0.999692
	Test subset	0.000019	2.36	0.999512
	Whole databank	0.000017	2.41	0.999664
Cascade feedforward neural network	Train subset	0.002319	2.67	0.999774
	Test subset	0.013574	2.41	0.999156
	Whole databank	0.004628	2.46	0.999596
Radial basis function neural network	Train subset	0.002413	3.54	0.999767
	Test subset	0.023266	2.88	0.998812
	Whole databank	0.006692	3.01	0.999439
Generalized regression neural network	Train subset	3.194334	12.82	0.639363
	Test subset	6.687986	15.05	0.386423
	Whole databank	3.911239	14.59	0.579964

Table 6.
Comparison of performances of different ANN models.

have single hidden layer with 10 neurons. The multi-layer perceptron, cascade feedforward, radial basis function, and generalized regression approach shows AARDs of 2.41, 2.46, 3.01, and 14.59% for prediction of whole experimental databank, respectively. It is clear that the MLP model presents the smallest error (AARD% = 2.63) for training subset while the worst results for estimation of this dataset (AARD% = 12.82) was presented by the GR model. It is widely accepted that a GR approach in which hidden neurons equals with the number of training data-points can provide the best accuracy for estimation of any continuous function. The worst result that is provided by the GR neural network in this study may be associated with the discontinuity in the experimental data of convective HTC or/ and the number of 10 hidden neurons that is very low than its theoretical threshold. Comparison among the predictive performances of these four ANN paradigms reveals that the MLP approach simply outperforms other ANN model for predicting the experimental values of convective HTC of both pure fluids and nanofluids. Therefore, a single hidden layer MLP model with 10 neurons that present the best performance for estimation of the convective HTC is considered as the best neural network model.

Figure 8 depicts change of the MSE for training dataset for the best MLP model. It is obvious that the MSE reaches relatively small value of 1.6×10^{-5} after 1000 iterations. Consequently, it can be claimed that the learning procedure of the MLP model was successful and this trained model can be used for more analyses.

3.2.3 Evaluation of the performance of developed MLP model

Figure 9 illustrates the plot of training (square symbols) and testing groups (spheres symbols) for experimental data of convective HTC as function of predicted values by the best MLP model. The most exact predictions, i.e., (pre-dictions = experimental) is depicted by the dashed 45° line. The relatively slight deviations from the dashed line justify that MLP predictions are properly mapped on their associated experimental data.
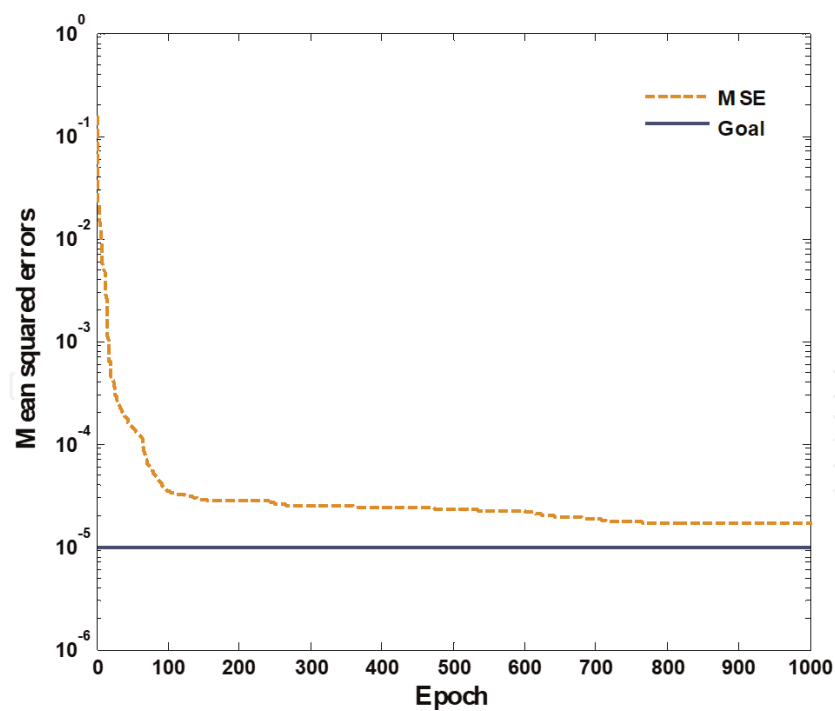
Figure 8.
MSE variation versus epoch for optimal MLP model predicting heat transfer coefficient, solid line represents goal while dashed line is training.
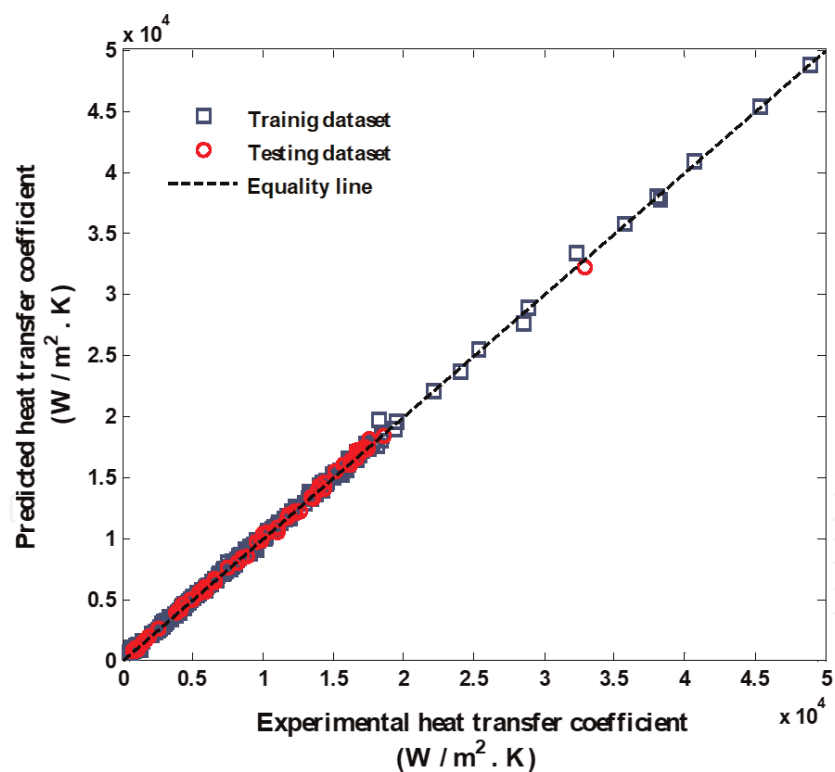

Figure 9.
Schematic presentation of the proposed optimal MLP network capability in estimating the experimental heat transfer coefficient over training + testing datasets.

Our developed MLP model with optimum configuration shows regression coefficient of 0.999692 for the prediction of training dataset of convective HTCs. It also presented the MSE and AARD of 1.6×10^{-5} and 2.63% for training group, respectively. Moreover, it can predict the testing dataset with impressing R^2 = 0.999512, AARD = 2.365%, and MSE = 1.9×10^{-5}.
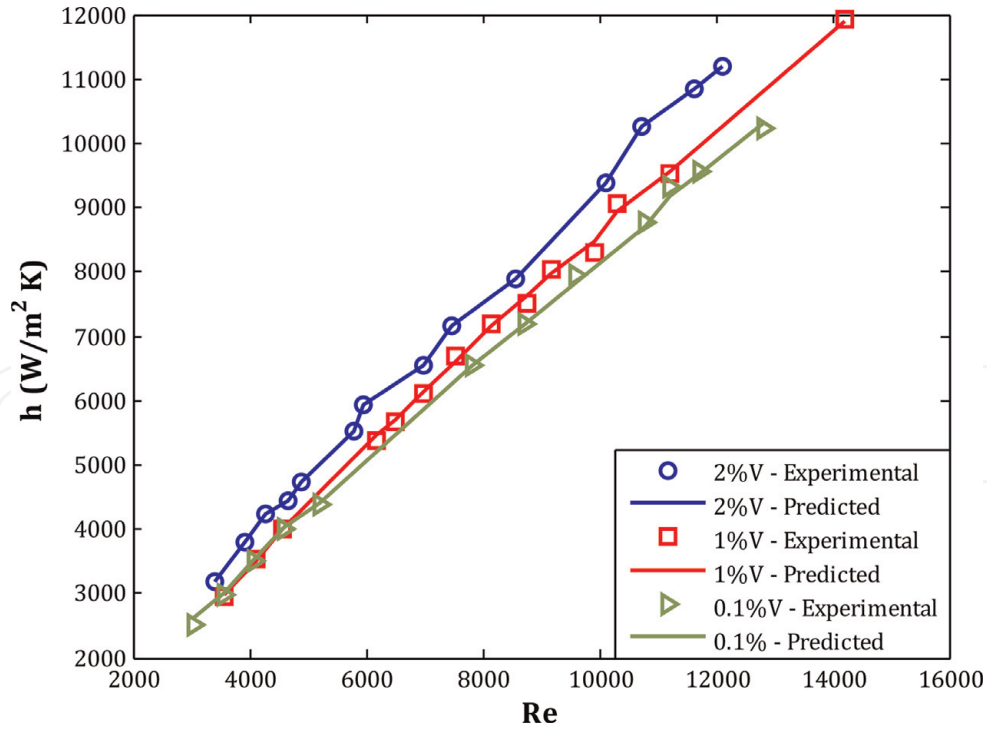
Figure 10.
Effect of particle volumetric concentration on the convective heat transfer coefficient, closed circles represent experimental data and solid lines are the results of MLP model.

The effect of particle volumetric concentration on the convective heat transfer coefficient of Al_2O_3 nanofluid flowing through a circular tube is investigated in **Figure 10**. It is obvious that the convective HTC increases by increasing the nanoparticle concentration in base fluid. Moreover, the level of this increase for higher Reynolds number (higher velocity) is more substantial. This behavior may be explained by more turbulence movement of nanoparticles in higher Reynolds number. High concentration of nanoparticles in base fluids is a factor that is responsible for increasing the interface between fluid and particles and enhancement of heat transfer rate.

Result of another analysis that is performed to investigate an effect of type of nanoparticles including Al_2O_3, CuO, and SiO_2 on HTC of water-based nanofluids is shown in **Figure 11**. It can be simply understood that the convective HTC of water-based nanofluids is remarkably higher than the pure water. Chaotic movement of nanoparticles as well as higher thermal conductivity of nanofluids may be responsible for higher heat transfer rate of nanofluids than the pure base fluids. A significant difference between convective HTC of the considered nanoparticles can also be seen in **Figure 11**. A possible reason for this difference may be the difference in thermophysical properties of nanoparticles. Since the metallic particles (CuO and Al_2O_3) have higher density, higher thermal conductivity in comparison with non-metallic particles (SiO_2), a higher heat transfer coefficients are provided in the presence of metallic particles.

3.3 Viscosity

Viscosity is one of the most important properties of fluids/nanofluids that directly influences on their heat transfer applications and flow behavior. Accurate and reliable estimation of viscosity is required for calculation of convection HTC, Prandtl, and Reynolds numbers, amount of pressure drop, and theoretical power of pump.

3.3.1 Experimental databank

Both empirical correlations [57, 69–77] and published literature data [24, 78–88] approved that the dynamic viscosity of nanofluids is essentially dependent on chemistry of base liquid, characteristics of nanoparticle, and ranges of operating conditions. Considering the corresponding state theory, the base fluids are tried to be introduced based on their critical temperature, critical pressure, and acentric factor [89]. Numerical values of these fundamental parameters for different base liquids are reported in **Table** 7. It is worthy to be noted that critical temperature, critical pressure, and acentric factor for mixtures of water-ethylene glycol are obtained using the Kay's mixing rule [90].

Temperature is likely the most important operating condition that could change the viscosity of both pure fluids and nanofluids. For incorporation, the effect of
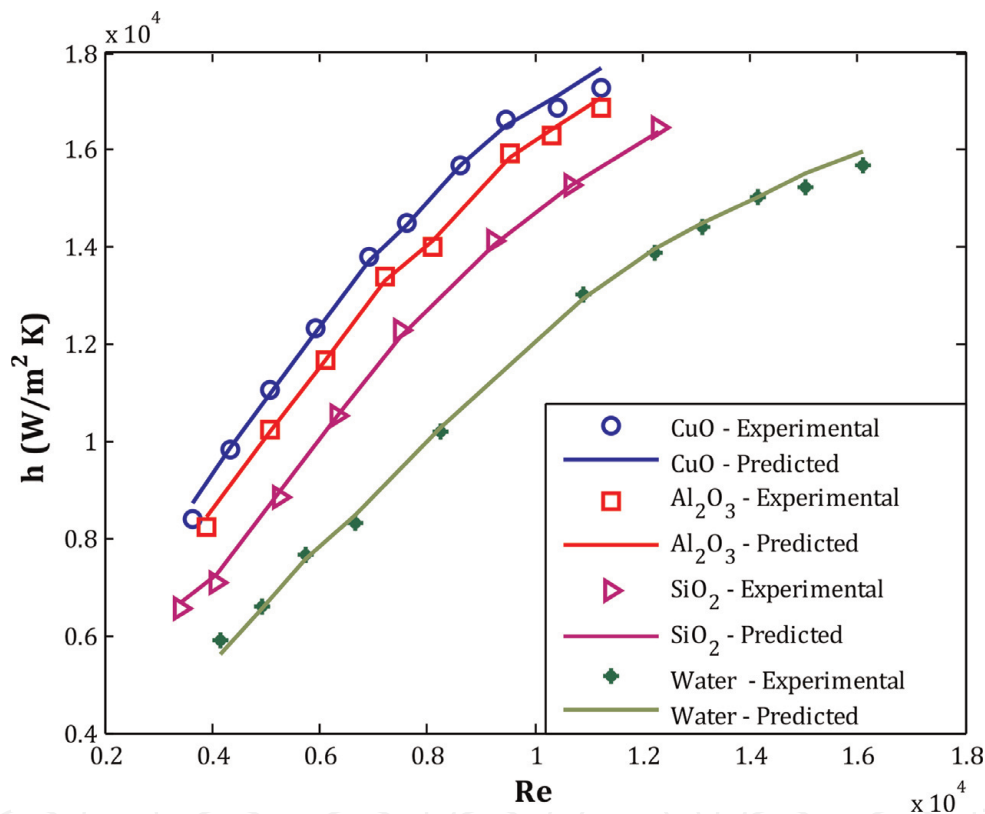

Figure 11.
Effect of particle type on the heat transfer coefficient, closed circles represent experimental data and solid lines are the results of MLP model.

Liquid	Pc (MPa)	Tc (K)	Acentric factor
Water	22.06	647.1	0.343
Propylene Glycol (PG)	6.04	626	1.102
EG/water (60/40)	17.71	669.1	0.387
EG/Water (45/55)	19.31	661	0.371
EG/Water (40/60)	19.73	658.9	0.366
Ethylene glycol (EG)	7.71	719.7	0.487

Table 7.
Acentric factor and critical properties of the pure base liquids.

Liquid	Dp (nm)	Vp (%)	Temperature (K)	Viscosity (mPa.s)	No. of data	Reference
Water	47	1–9.4	294–343	0.43–4.91	81	[80]
Water	13	1.34–2.78	293–345	0.63–2.49	14	[81]
Water	30	0.01–0.3	294–312	0.66–1.00	114	[82]
Water	33	1–2	293–313	0.65–1.09	10	[83]
Ethylene glycol (EG)	8–43	0.5–6.6	283–323	7.51–81.51	96	[78]
Ethylene glycol (EG)	10	1–5	298–328	8.14–37.28	21	[79]
Propylene glycol (PG)	27–50	0.5–3	303–333	7.9–38.6	36	[85]
EG/water (20/80)	36	0–1.5	273–333	0.59–4.6	89	[84]
EG/water (40/60)	36	0–1.5	273–333	0.96–13.64	90	[84]
EG/water(45/55)	30	0–2	283–333	1.54–11.08	33	[24]
EG/water(60/40)	36	0–1.5	273–333	1.5–35.35	90	[84]
Overall ranges	8–50	0–9.4	273–345	0.43–81.51	674	[24, 78–85]

Table 8.
Brief description of collected experimental datasets for dynamic viscosity of alumina-based nanofluids.

nanoparticles, their diameter, and volumetric concentration (Vp) in liquid are also regarded as independent factors. A brief description of experimental databank including independent and dependent variable(s), their associated ranges, and number of collected datasets from different literatures are presented in **Table 8** [24, 78–85].

Table 8 states that our experimental databank for viscosity of different base fluids - alumina nanoparticle has 674 data-points. The databank includes seven different base liquids in temperature range of 273–345 K. These base liquids may have up to 9.4 volume percent of alumina nanoparticle with diameter of 8 to 50 nm. The dynamic viscosity of the considered nanofluids varies from 0.43 to 81.51 mPa.

3.3.2 ANN model development

Similar to two previous modelings, the best structure of MLP model is selected through trial and error analyses. The results of this trial and error procedure on the number of hidden neurons for the MLP network were reported in **Table 9**. Different MLP models having 1 to 15 hidden neurons were developed, trained, tested, and their performances were evaluated. The smallest number of hidden neurons that provides an acceptable accuracy is often selected as an optimum structure.

Table 9 clearly shows that performance of the MLP model got better by increasing the number of hidden neuron up to 14. After that, a relatively worse result is obtained for testing subset even by spending higher computational time and effort. Thus, a two-layer MLP approach constituting of 14 hidden neurons (the bold rows) was selected as the best topology for prediction of dynamic viscosity of dispersion of alumina nanoparticles in different base fluids. It is obvious that this MLP model predicted whole of the experimental data-points with R^2 of 0.99947, MSE of 0.1442, AARD of 4.13%, and RMSE of 0.3797.

It is common to compare the predictive performance of various types of ANN and find the best one in terms of some statistical indices. **Table 10** summarizes the

Number of hidden neurons	Database	Sensitivity accuracy analyses			
		AARD%	MSE	R^2	RMSE
2	Training	24.62	3.4708	0.98488	1.8630
	Testing	27.07	6.5978	0.99033	2.5686
	Overall	24.99	3.9394	0.98562	1.9848
4	Training	17.02	1.5977	0.99414	1.2640
	Testing	17.79	1.5941	0.99402	1.2626
	Overall	17.14	1.5972	0.99409	1.2638
6	Training	12.94	0.5584	0.99795	0.7473
	Testing	15.09	0.7587	0.99726	0.8710
	Overall	13.26	0.5884	0.99783	0.7671
8	Training	8.80	0.3267	0.99876	0.5715
	Testing	10.79	1.0471	0.99723	1.0233
	Overall	9.10	0.4346	0.99841	0.6593
9	Training	8.20	0.1343	0.99946	0.3665
	Testing	9.64	0.2289	0.99961	0.4784
	Overall	8.41	0.1485	0.99946	0.3853
10	Training	6.55	0.1183	0.99956	0.3440
	Testing	7.81	0.1864	0.99940	0.4318
	Overall	6.74	0.1285	0.99953	0.3585
11	Training	6.53	0.1263	0.99956	0.3554
	Testing	8.19	1.7631	0.99352	1.3278
	Overall	6.78	0.3716	0.99866	0.6096
12	Training	5.63	0.0906	0.99968	0.3011
	Testing	6.04	0.2209	0.99891	0.4700
	Overall	5.69	0.1102	0.99959	0.3319
13	Training	4.38	0.0859	0.99969	0.2931
	Testing	6.30	0.3259	0.99869	0.5709
	Overall	4.67	0.1219	0.99955	0.3491
14	**Training**	**4.11**	**0.1025**	**0.99962**	**0.3202**
	Testing	**4.22**	**0.3804**	**0.99867**	**0.6167**
	Overall	**4.13**	**0.1442**	**0.99947**	**0.3797**
15	Training	4.72	0.0799	0.99971	0.2827
	Testing	5.91	0.3091	0.99861	0.5560
	Overall	4.90	0.1143	0.99958	0.3381

The bold values indicate the best obtained results for the considered AI models.

Table 9.
Trial and error procedure for finding the best structure for MLPNN model.

obtained results by the best topology of the CFF, MLP, RBF, and least square support vector machines (LS-SVM) models for training, testing, and overall datasets in term of AARD%, MSE, R^2, and RMSE.

Focusing on reported results in **Table 10** clearly confirms that the MLP neural network provides the best predictive performance for prediction of dynamic viscosity of different Al_2O_3-based nanofluids. Since, it outperforms other

AI model	Dataset	AARD%	MSE	R^2	RMSE
MLP	**Training stage**	**4.11**	**0.1025**	**0.99962**	**0.3202**
	Testing stage	**4.22**	**0.3804**	**0.99867**	**0.6167**
	Overall data	**4.13**	**0.1442**	**0.99947**	**0.3797**
CFF	Training stage	4.13	0.0989	0.99965	0.3144
	Testing stage	4.74	0.1850	0.99911	0.4302
	Overall data	4.22	0.1118	0.99959	0.3343
LS-SVM	Training stage	6.33	0.0791	0.99971	0.2812
	Testing stage	10.27	2.5489	0.99073	1.5965
	Overall data	6.92	0.4492	0.99834	0.6702
RBF	Training stage	57.91	5.599	0.9759	2.366
	Testing stage	50.58	14.425	0.9753	3.798
	Overall data	56.81	6.922	0.9745	2.631

The bold values indicate the best obtained results for the considered AI models.

Table 10.
Comparison among the capabilities of different AI approaches in prediction of viscosity of nanofluids.
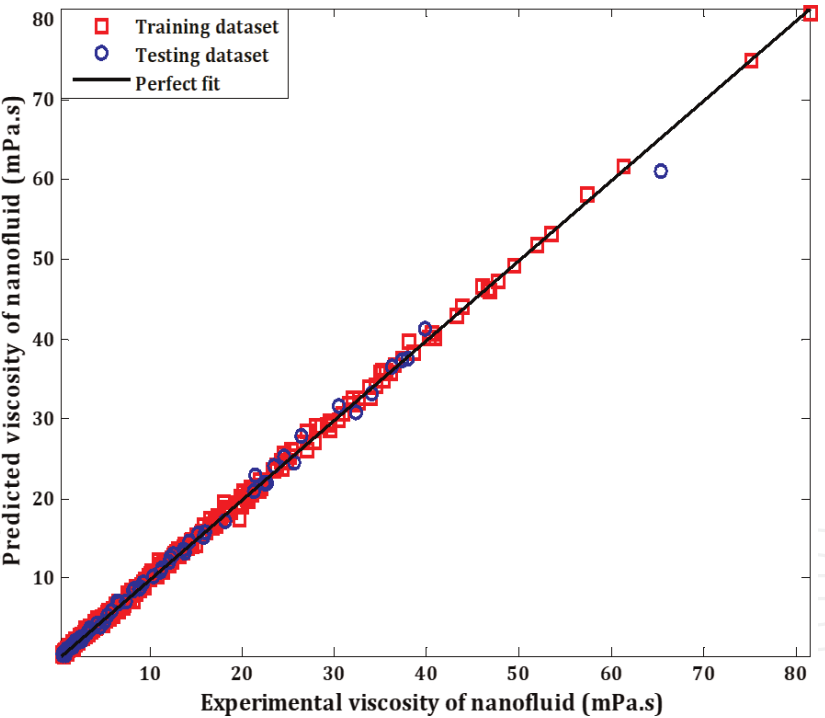

Figure 12.
Performance of the best AI model for estimation of viscosity of alumina-based nanofluids.

considered AI approaches; it therefore can be regarded as the best AI approach for considered task.

3.3.3 Evaluation the ANN model performances

Plot of estimated viscosity for different nanofluids by the optimum MLP network with respect to their associated experimental data for training and testing datasets are depicted in **Figure 12**. Aggregation of the symbols for training as well as testing subsets around the 45° solid line approves that the developed MLP model is a

Experimental data	Einstein [69]	Brinkman [70]	Frankel and Acrivos [71]	Nguyen et al. [72]	Batchelor [73]	Maiga et al. [74]	Thomas and Muthukumar [75]	Rea et al. [76]	Chandrasekar et al. [57]	Heyhat et al. [77]
Ethylene glycol [78]	24.20	23.98	94.03	27.84	23.90	11.56	23.96	54.46	27.80	34.40
Ethylene glycol [79]	39.37	39.15	82.83	42.93	39.06	26.59	39.13	38.38	42.90	24.95
Water [80]	33.80	33.17	180.63	39.36	32.97	11.92	33.12	383.73	39.31	168.62
Water [81]	44.63	44.53	165.32	47.17	44.48	37.11	44.52	11.04	47.14	16.15
Water [82]	2.97	2.97	173.55	3.23	2.97	2.45	2.97	1.26	3.23	1.32
Water [83]	7.24	7.18	337.49	8.73	7.16	5.80	7.18	34.77	8.70	29.54
EG/water (20/80) [84]	10.18	10.16	286.76	11.61	10.15	7.08	10.16	6.66	11.60	5.35
EG/water (40/60) [84]	27.91	27.91	252.39	28.17	27.91	27.68	27.91	31.24	28.16	30.32
EG/water(45/55) [24]	35.87	35.84	147.00	36.90	35.83	33.14	35.84	24.17	36.89	25.70
EG/water(60/40) [84]	38.94	38.93	120.06	39.72	38.92	37.10	38.93	31.12	39.72	32.01
Propylene glycol [85]	15.90	15.74	273.78	19.51	15.68	7.06	15.73	37.10	19.48	29.47
Overall AARD%	24.20	23.02	180.25	25.14	22.97	16.76	23.01	68.40	25.12	38.80

Table 11.
Provided AARD% for prediction of experimental datasets by different empirical correlations.

Experimental data	MLP	CFF	LS-SVM	Correlation*	RBF
Ethylene glycol [78]	1.94	1.67	2.28	11.56	7.56
Ethylene glycol [79]	3.61	3.53	2.72	24.95	12.34
Water [80]	2.82	4.58	4.59	11.92	170.58
Water [81]	7.65	5.93	15.68	11.04	100.90
Water [82]	2.59	1.19	8.94	1.26	28.11
Water [83]	29.02	11.26	35.64	5.8	53.48
EG/water (20/80) [84]	5.96	6.30	11.71	5.35	84.15
EG/water (40/60) [84]	4.53	6.12	8.16	27.68	62.74
EG/water (45/55) [24]	5.42	5.43	7.10	24.17	35.03
EG/water (60/40) [84]	4.75	6.63	4.29	31.12	38.29
Propylene glycol [85]	1.56	0.90	0.33	7.06	16.70
Overall AARD%	4.13	4.24	6.92	14.50	56.81

The best obtained result among all of the considered empirical correlations.

Table 12.
Provided AARD% for prediction of experimental datasets by different methodologies.

practical tool for accurate estimation of the dynamic viscosity of different Al_2O_3-based nanofluids in wide ranges of operating conditions.

In this section, some analyses are performed to compare predictive accuracy of the proposed AI model with 10 well-known empirical correlations in literature [57, 69–77]. The obtained AARD% values by the considered empirical correlations for prediction of dynamic viscosity of nanofluids are reported in **Table 11**. It is obvious that the proposed model by Maiga et al. [74] is the most accurate empirical correlation, while the model developed by Frankel and Acrivos [71] presents the worst results. The earlier one has an AARD of 16.76%, while the later shows the AARD of 180.25%.

The obtained values for AARD by various AI models and the best obtained results by the considered empirical correlations are summarized in **Table 12**. It can be easily understood that the best results among 10 empirical correlations only outperforms the RBF model and predictive performance of other AI models is more better than the empirical correlations.

4. Conclusions

Nanofluids are new and high-tech class of operating fluids that recently found high popularity in the field of heat transfer equipment. In spite of both practical and potential application of nanofluids, three developed no accurate correlations for estimation of thermophysical properties of nanofluids in wide ranges of conditions. In this chapter, the focus was concentrated on estimation of conduction heat transfer coefficient, convective HTC, and viscosity of different nanofluids by four different artificial neural networks. MLP, RBF, CFF, and GR are the types of ANN methodology that are employed for these estimations. The best structures of ANN models are determined, their predictive performances are compared and the best one is presented. Some statistical error indices including MSE, RMSE, AARD%, and R^2 are used for evaluation of the accuracy of the ANN models. Results confirm that

ANN models capable of accurate estimation of thermophysical properties of nanofluids and show better performances than the available empirical correlations.

Acronyms and abbreviations

ANN	artificial neural network
MSE	mean square errors
RMSE	root mean square errors
AARD%	average absolute relative deviation percent
MLP	multilayer perceptron
CFF	cascade feedforward
RBF	radial basis function
GR	generalized regression
TCR	thermal conductivity ratio
HTC	heat transfer coefficient
EG	ethylene glycol
PG	propylene glycol
LS-SVM	least square support vector machines

Appendices and nomenclature

R^2	regression coefficient
w	weight
b	bias
out	perceptron's output
f	activation function
Ind	number of dimensions of independent variable
Dep	number of dimensions of dependent variable
N	number of experimental data
D	value of dependent variable
Exp	experimental data
Cal	calculated values
Dp	diameter of nanoparticle
T	temperature
Mw	molecular weight
Vf	volume fraction of nanoparticle
ω	acentric factor
Pc	critical pressure of base fluids
Tc	critical temperature of base fluids
Re	Reynolds number
h	convective heat transfer coefficient
Vp	volume percent of nanoparticle

Author details

Behzad Vaferi
Department of Chemical Engineering, Shiraz Branch, Islamic Azad University,
Shiraz, Iran

*Address all correspondence to: behzad.vaferi@gmail.com

IntechOpen

References

[1] Ghanem A, Habchi C, Lemenand T, Della Valle D, Peerhossaini H. Energy efficiency in process industry–high-efficiency vortex (HEV) multifunctional heat exchanger. Renewable Energy. 2013;**56**:96-104

[2] Marques C, Kelly KW. Fabrication and performance of a pin fin micro heat exchanger. Journal of Heat Transfer. 2004;**126**:434-444

[3] Huminic G, Huminic A. Application of nanofluids in heat exchangers: A review. Renewable and Sustainable Energy Reviews. 2012;**16**:5625-5638

[4] Mondragón R, Segarra C, Martínez-Cuenca R, Juliá JE, Jarque JC. Experimental characterization and modeling of thermophysical properties of nanofluids at high temperature conditions for heat transfer applications. Powder Technology. 2013;**249**:516-529

[5] Xiao B, Yang Y, Chen L. Developing a novel form of thermal conductivity of nanofluids with Brownian motion effect by means of fractal geometry. Powder Technology. 2013;**239**:409-414

[6] Salimi-Yasar H, Heris SZ, Shanbedi M, Amiri A, Kameli A. Experimental investigation of thermal properties of cutting fluid using soluble oil-based TiO_2 nanofluid. Powder Technology. 2017;**310**:213-220

[7] Wang X, Xu X, Choi SUS. Thermal conductivity of nanoparticle-fluid mixture. Journal of Thermophysics and Heat Transfer. 1999;**13**:474-480

[8] Hwang Y, Lee JK, Jeong YM, Cheong SI, Ahn YC, Kim SH. Production and dispersion stability of nanoparticles in nanofluids. Powder Technology. 2008;**186**:145-153

[9] Lee S, Choi SS, Li SA, Eastman JA. Measuring thermal conductivity of fluids containing oxide nanoparticles. Journal of Heat Transfer. 1999;**121**: 280-289

[10] Trisaksri V, Wongwises S. Critical review of heat transfer characteristics of nanofluids. Renewable and Sustainable Energy Reviews. 2007;**11**:512-523

[11] Sharma P, Baek IH, Cho T, Park S, Lee KB. Enhancement of thermal conductivity of ethylene glycol based silver nanofluids. Powder Technology. 2011;**208**:7-19

[12] Saeedinia M, Akhavan-Behabadi MA, Nasr M. Experimental study on heat transfer and pressure drop of nanofluid flow in a horizontal coiled wire inserted tube under constant heat flux. Experimental Thermal and Fluid Science. 2012;**36**:158-168

[13] Choi SUS. Enhancing thermal conductivity of fluids with nanoparticles. In: Siginer DA, Wang HP, editors. Developments and Applications of Non-Newtonian Flows. Vol. 66. New York: ASME; 1995. pp. 99-105

[14] Sundar LS, Sharma KV, Naik MT, Singh MK. Empirical and theoretical correlations on viscosity of nanofluids: A review. Renewable and Sustainable Energy Reviews. 2013;**25**: 670-686

[15] Chiam HW, Azmi WH, Usri NA, Mamat R, Adam NM. Thermal conductivity and viscosity of Al_2O_3 nanofluids for different based ratio of water and ethylene glycol mixture. Experimental Thermal and Fluid Science. 2017;**81**:420-429

[16] Ariana MA, Vaferi B, Karimi G. Prediction of thermal conductivity of alumina water-based nanofluid by artificial neural networks. Powder Technology. 2015;**278**:1-10

[17] Yang L, Du K, Zhang X. A theoretical investigation of thermal conductivity of nanofluids with particles in cylindrical shape by anisotropy analysis. Powder Technology. 2017;**314**:328-338

[18] Yang L, Xu J, Du K, Zhang X. Recent developments on viscosity and thermal conductivity of nanofluids. Powder Technology. 2017;**317**:348-369

[19] Choi SUS. Enhancing thermal conductivity of fluids with nanoparticles. In: Proceedings of the ASME International Mechanical Engineering Congress and Exposition, San Francisco. 1995. pp. 99-105

[20] Goshayeshi HR, Safaei MR, Goodarzi M, Dahari M. Particle size and type effects on heat transfer enhancement of Ferro-nanofluids in a pulsating heat pipe. Powder Technology. 2016;**301**:1218-1226

[21] Duangthongsuk W, Wongwises S. An experimental study on the heat transfer performance and pressure drop of TiO_2-water nanofluids flowing under a turbulent flow regime. International Journal of Heat and Mass Transfer. 2010;**53**:334-344

[22] Nguyen CT, Roy G, Gauthier C, Galanis N. Heat transfer enhancement using Al_2O_3–water nanofluid for an electronic liquid cooling system. Applied Thermal Engineering. 2007;**27**(8–9):1501-1506

[23] Mallick SS, Mishra A, Kundan L. An investigation into modelling thermal conductivity for alumina–water nanofluids. Powder Technology. 2013;**233**:234-244

[24] Yu W, Xie H, Li Y, Chen L, Wang Q. Experimental investigation on the heat transfer properties of Al_2O_3 nanofluids using the mixture of ethylene glycol and water as base fluid. Powder Technology. 2012;**230**:14-19

[25] Gurney K. Neural networks for perceptual processing: From simulation tools to theories. Philosophical Transactions of the Royal Society B. 2007;**362**(1479):339-353

[26] Ghaffarian N, Eslamloueyan R, Vaferi B. Model identification for gas condensate reservoirs by using ANN method based on well test data. Journal of Petroleum Science and Engineering. 2014;**123**:20-29

[27] Vaferi B, Eslamloueyan R, Ghaffarian N. Hydrocarbon reservoir model detection from pressure transient data using coupled artificial neural network-wavelet transform approach. Applied Soft Computing. 2016;**47**:63-75

[28] Demuth HB, Beale MH, De Jess O, Hagan M. Neural Network Design. Oklahoma: Martin Hagan; 2014

[29] Fahlman S, Lebiere C. The cascade-correlation learning architecture. In: Touretzky D, editor. Advances in Neural Information Processing Systems 2. San Mateo: Denver, CO. Morgan Kaufmann Publishers; 1990:524-532

[30] Lashkarbolooki M, Vaferi B, Shariati A, Hezave AZ. Investigating vapor-liquid equilibria of binary mixtures containing supercritical or near-critical carbon dioxide and a cyclic compound using cascade neural network. Fluid Phase Equilibria. 2013;**343**:24-29

[31] Cheng G, Zhou J, Zhang XJ, Zhang ZJ. A daily load forecasting method based on cascaded back propagation and radial basis function neural networks. Power System Technology. 2009;**33**:101-105

[32] Chen S, Cowan CFN, Grant PM. Orthogonal least squares learning algorithm for radial basis function networks. IEEE Transactions on Neural Networks. 1991;**2**:302-309

[33] Broomhead DS, Lowe D. Multivariable functional interpolation and adaptive networks. Complex Systems. 1988;**2**:321-355

[34] Zhao N, Wen X, Yang J, Li S, Wang Z. Modeling and prediction of viscosity of water-based nanofluids by radial basis function neural networks. Powder Technology. 2015;**281**:173-183

[35] Specht DF. A general regression neural network. IEEE Transactions on Neural Networks. 1991;**2**:568-578

[36] Maxwell JC. A Treatise on Electricity and Magnetism. London: Oxford University Press; 1873

[37] Xie H, Wang J, Xi T, Liu Y, Ai F, Wu Q. Thermal conductivity enhancement of suspensions containing nanosized alumina particles. Journal of Applied Physics. 2002;**91**:4568-4572

[38] Kahani M, Zeinali Heris S, Mousavi SM. Comparative study between metal oxide nanopowders on thermal characteristics of nanofluid flow through helical coils. Powder Technology. 2013;**246**:82-92

[39] Das SK, Putra N, Thiesen P, Roetzel W. Temperature dependence of thermal conductivity enhancement for Nanofluids. Journal of Heat Transfer. 2003;**125**:567-574

[40] Yoo DH, Hong KS, Yang HS. Study of thermal conductivity of nanofluids for the application of heat transfer fluids. Thermochimica Acta. 2007;**455**: 66-69

[41] Hatami M, Sheikholeslami M, Ganji DD. Laminar flow and heat transfer of nanofluid between contracting and rotating disks by least square method. Powder Technology. 2014;**253**:769-779

[42] Hamilton RL, Crosser OK. Thermal conductivity of heterogeneous two component systems. Industrial & Engineering Chemistry Fundamentals. 1962;**1**:187-191

[43] Masuda H, Ebata A, Teramae K, Hishinuma N. Alteration of thermal conductivity and viscosity of liquid by dispersing ultra-fine particles dispersion of Al_2O_3, SiO_2 and TiO_2 ultra-fine particles. Netsu Bussei. 1993;**7**:227-233

[44] Murshed SMS, Leong KC, Yang C. Enhanced thermal conductivity of TiO_2-water based nanofluids. International Journal of Thermal Sciences. 2005;**44**: 367-373

[45] Chon CH, Kihm KD, Lee SP, Choi SUS. Empirical correlation finding the role of temperature and particle size for nanofluid (Al_2O_3) thermal conductivity enhancement. Applied Physics Letters. 2005;**87**:153107-1-153107-3

[46] Li CH, Peterson GP. Experimental investigation of temperature and volume fraction variations on the effective thermal conductivity of nanoparticle suspensions (nanofluids). Journal of Applied Physics. 2006;**99**: 084314-1-084314-8

[47] Murshed SMS, Leong KC, Yang C. Investigations of thermal conductivity and viscosity of nanofluids. International Journal of Thermal Sciences. 2008;**47**:560-568

[48] Teng TP, Hung YH, Teng TC, Mo HE, Hsu HG. The effect of alumina/water nanofluid particle size on thermal conductivity. Applied Thermal Engineering. 2010;**30**:2213-2218

[49] Mintsa HA, Roy G, Nguyen CT, Doucet D. New temperature dependent thermal conductivity data for water-based nanofluids. International Journal of Thermal Sciences. 2009;**48**:363-371

[50] Longo GA, Zilio C. Experimental measurement of thermophysical

properties of oxide–water nano-fluids down to ice-point. Experimental Thermal and Fluid Science. 2011;**35**: 1313-1324

[51] Timofeeva EV, Gavrilov AN, McCloskey JM, Tolmachev YV, Sprunt S, Lopatina LM, et al. Thermal conductivity and particle agglomeration in alumina nanofluids: Experiment and theory. Physical Review E. 2007;**76**: 061203-1-061203-16

[52] Zhang X, Gu H, Fujii M. Effective thermal conductivity and thermal diffusivity of nanofluids containing spherical and cylindrical nanoparticles. Experimental Thermal and Fluid Science. 2007;**31**: 593-599

[53] Yiamsawasd T, Dalkilic AS, Wongwises S. Measurement of the thermal conductivity of titania and alumina nanofluids. Thermochimica Acta. 2012;**545**:48-56

[54] Buschmann MH. Thermal conductivity and heat transfer of ceramic nanofluids. International Journal of Thermal Sciences. 2012;**62**: 19-28

[55] Beck M, Yuan Y, Warrier P, Teja A. The effect of particle size on the thermal conductivity of alumina nanofluids. Journal of Nanoparticle Research. 2009; **11**:1129-1136

[56] Beck M, Yuan Y, Warrier P, Teja A. The thermal conductivity of alumina nanofluids in water, ethylene glycol, and ethylene glycol + water mixtures. Journal of Nanoparticle Research. 2010; **12**:1469-1477

[57] Chandrasekar M, Suresh S, Chandra Bose A. Experimental investigations and theoretical determination of thermal conductivity and viscosity of Al_2O_3/ water nanofluid. Experimental Thermal and Fluid Science. 2010;**34**: 210-216

[58] Li CH, Peterson GP. The effect of particle size on the effective thermal conductivity of Al_2O_3-water nanofluids. Journal of Applied Physics. 2007;**101**: 044312-1-044312-5

[59] Canakci A, Ozsahin S, Varol T. Modeling the influence of a process control agent on the properties of metal matrix composite powders using artificial neural networks. Powder Technology. 2012;**228**:26-35

[60] Yu W, Choi SUS. The role of interfacial layers in the enhanced thermal conductivity of Nanofluids: A renovated Maxwell model. Journal of Nanoparticle Research. 2003;**5**: 167-171

[61] Xie H, Fujii M, Zhang X. Effect of interfacial nanolayer on the effective thermal conductivity of nanoparticle-fluid mixture. International Journal of Heat and Mass Transfer. 2005;**48**: 2926-2932

[62] Nan CW, Birringer R, Clarke DR, Gleiter H. Effective thermal conductivity of particulate composites with interfacial thermal resistance. Journal of Applied Physics. 1997;**81**: 6692-6699

[63] Xuana Y, Roetzel W. Conceptions for heat transfer correlation of nanofluids. International Journal of Heat and Mass Transfer. 2000;**43**: 3701-3707

[64] Anoop KB, Sundararajan T, Das SK. Effect of particle size on the convective heat transfer in nanofluid in the developing region. International Journal of Heat and Mass Transfer. 2009;**52**: 2189-2195

[65] Vajjha RS, Das DK, Kulkarni DP. Development of new correlations for convective heat transfer and friction factor in turbulent regime for nanofluids. International Journal of Heat and Mass Transfer. 2010;**53**:4607-4618

[66] Heyhat MM, Kowsary F, Rashidi AM, Alem Varzane Esfehani S, Amrollahi A. Experimental investigation of turbulent flow and convective heat transfer characteristics of alumina water nanofluids in fully developed flow regime. International Communications in Heat and Mass Transfer. 2012;**39**: 1272-1278

[67] SyamSundar L, Naik MT, Sharma KV, Singh MK, Siva Reddy TC. Experimental investigation of forced convection heat transfer and friction factor in a tube with Fe_3O_4 magnetic nanofluid. Experimental Thermal and Fluid Science. 2012;**37**:65-71

[68] Bayat J, Nikseresht AH. Thermal performance and pressure drop analysis of nanofluids in turbulent forced convective flows. International Journal of Thermal Sciences. 2012;**60**:236-243

[69] Einstein A. Eine neue bestimmung der moleküldimensionen. Annalen der Physik. 1906;**324**:289-306

[70] Brinkman HC. The viscosity of concentrated suspensions and solution. The Journal of Chemical Physics. 1952;**20**:571-581

[71] Frankel NA, Acrivos A. On the viscosity of a concentrate suspension of solid spheres. Chemical Engineering Science. 1967;**22**:847-853

[72] Nguyen CT, Desgranges F, Galanis N, Roy G, Maré T, Boucher S, et al. Viscosity data for Al_2O_3 - water nanofluid - hysteresis: Is heat transfer enhancement using nanofluids reliable? International Journal of Thermal Sciences. 2008;**47**:103-111

[73] Batchelor GK. The effect of Brownian motion on the bulk stress in a suspension of spherical particles. Journal of Fluid Mechanics. 1977;**83**:97-117

[74] Maiga SEB, Nguyen CT, Galanis N, Roy G. Heat transfer behaviours of nanofluids in a uniformly heated tube. Superlattices and Microstructures. 2004;**35**:543-557

[75] Thomas CU, Muthukumar M. Three-body hydrodynamic effects on viscosity of suspensions of spheres. The Journal of Chemical Physics. 1991;**94**: 5180-5189

[76] Rea U, McKrell T, Hu LW, Buongiorno J. Laminar convective heat transfer and viscous pressure loss of alumina-water and zirconia-water nanofluids. International Journal of Heat and Mass Transfer. 2009;**52**: 2042-2048

[77] Heyhat MM, Kowsary F, Rashidi AM, Memenpour MH, Amrollahi A, Momenpour MH. Experimental investigation of laminar convective heat transfer and pressure drop of water-based Al_2O_3 nanofluids in fully developed flow regime. Experimental Thermal and Fluid Science. 2013;**44**:483-489

[78] Pastoriza-Gallego MJ, Lugo L, Legido JL, Piñeiro MM. Thermal conductivity and viscosity measurements of ethylene glycol-based Al_2O_3 nanofluids. Nanoscale Research Letters. 2011;**6**:1-11

[79] Hachey MA, Nguyen CT, Galanis N, Popa CV. Experimental investigation of Al_2O_3 nanofluids thermal properties and rheology - effects of transient and steady-state heat exposure. International Journal of Thermal Sciences. 2014;**76**:155-167

[80] Nguyen CT, Desgranges F, Roy G, Galanis N, Mare T, Boucher S, et al. Temperature and particle-size dependent viscosity data for water-based nanofluids – Hysteresis phenomenon. International Journal of Heat and Fluid Flow. 2007;**28**:1492-1506

[81] Pak BC, Cho YI. Hydrodynamic and heat transfer study of dispersed fluids

with submicron metallic oxide particles. Experimental Heat Transfer. 1998;**11**: 151-170

[82] Lee JH. Effective viscosities and thermal conductivities of aqueous nanofluids containing low volume concentrations of Al_2O_3 nanoparticles. International Journal of Heat and Fluid Flow. 2008;**51**:2651-2656

[83] Ho CJ, Wei LC, Li ZW. An experimental investigation of forced convective cooling performance of a microchannel heat sink with Al_2O_3/ water nanofluid. Applied Thermal Engineering. 2010;**30**:96-103

[84] Syam Sundar L, Venkata Ramana E, Singh MK, Sousa ACM. Thermal conductivity and viscosity of stabilized ethylene glycol and water mixture Al_2O_3 nanofluids for heat transfer applications: An experimental study. International Communications in Heat and Mass. 2014;**56**:86-95

[85] Prasher R, Song D, Wang J, Phelan P. Measurements of nanofluid viscosity and its implications for thermal applications. Applied Physics Letters. 2006;**89**:133108-133101

[86] Yang L, Yuhan H. Toward TiO_2 Nanofluids-part 1: Preparation and properties. Nanoscale Research Letters. 2017;**12**:417

[87] Yang L, Yuhan H. Toward TiO_2 Nanofluids—Part 2: Applications and challenges. Nanoscale Research Letters. 2017;**12**:446

[88] Yang L, Jiang W, Chen X, Du K. Dynamic characteristics of an environment-friendly refrigerant: Ammonia-water based TiO_2 nanofluids. International Journal of Refrigeration. 2017;**82**:366-380

[89] Carruth GF, Kobayashi R. Extension to low reduced temperatures of three-parameter corresponding states: Vapor pressures, enthalpies and entropies of vaporization, and liquid fugacity coefficients. Industrial and Engineering Chemistry Fundamentals. 1972;**11**: 509-517

[90] Poling BE, Prausnitz JM, O'connell JP. The Properties of Gases and Liquids. New York: Mcgraw-Hill; 2001